**J. Cent. South Univ.** (2022) 29: 1423−1436
**DOI:** https://doi.org/10.1007/s11771-022-5014-9

Springer

# Effect of Ni/Fe ratio on activation sintering and mechanical properties of molybdenum nickel iron alloy

LIU Jun-ru(刘俊汝), LI Zhi-bo(李志博), CHEN Ben(陈奔),
CHOU Kuo-chih(周国治), ZHANG Guo-hua(张国华)*

State Key Laboratory of Advanced Metallurgy, University of Science and Technology Beijing, Beijing 100083, China



**Abstract:** In order to improve the low ductility of the Mo-Ni alloy, Fe is added and the effects of Ni/Fe mass ratio on the densification behavior, microstructure evolution and mechanical properties of alloy were investigated. The experimental results show that when iron is added to 95Mo-5Ni alloy, the formation of brittle intermetallic phase $\delta$-MoNi at the grain boundary is avoided. Meanwhile, the grain growth of Mo is also effectively inhibited in the sintering process. However, the addition of iron reduces the degree of densification of alloy since the activation effect of Ni is superior to that of Fe. From the experimental results, it could be concluded that the maximum hardness and bending strength are achieved by 95Mo-1.5Ni-3.5Fe alloy, which are HV 614 and 741 MPa, respectively. Combined with the analyses of bending fracture mechanism, the improvement relative to Mo-Ni alloy is likely attributed to the inhibition of the brittle phase.

**Key words:** Mo-Ni-Fe alloy; sintering behavior; brittle phase; densification

**Cite this article as:** LIU Jun-ru, LI Zhi-bo, CHEN Ben, CHOU Kuo-chih, ZHANG Guo-hua. Effect of Ni/Fe ratio on activation sintering and mechanical properties of molybdenum nickel iron alloy [J]. Journal of Central South University, 2022, 29(5): 1423−1436. DOI: https://doi.org/10.1007/s11771-022-5014-9.

## 1 Introduction

As one of the most important refractory metals, molybdenum has a body-centered-cubic (bcc) crystal structure, high melting point (2610 °C), high-temperature strength, low coefficient of thermal expansion, good thermal conductivity and corrosion resistance. It has been widely applied in chemical, aerospace, energy and pharmaceutical industries [1−3]. Due to the high melting point characteristics of molybdenum and its alloys, the powder metallurgy (P/M) technology is always used. However, a very high sintering temperature (1800−2000 °C) and long sintering time are required, which leads to coarsening microstructure and deteriorates its mechanical performance [4, 5]. Two technologies are often employed to reduce sintering temperature, i. e., namely liquid phase sintering and solid state activated sintering [6−8]. GERMAN et al [9] used the transition metal as an activator to reduce sintering temperature by enhancing Mo diffusive transport through an additive-rich alloy layer at the grain boundaries. ZOVAS et al [10] found that the additions of Ni, Fe and Co can increase transport rates, lower sintering temperatures of Mo and enhance the densification of samples. Among these three elements, Ni had the most significant effect on the densification of samples. HOFMANN et al [11] revealed that the oxygen content of molybdenum

**Foundation item:** Project(51734002) supported by the National Natural Science Foundation of China
**Received date:** 2021-04-20; **Accepted date:** 2021-09-03
**Corresponding author:** ZHANG Guo-hua, PhD, Professor; E-mail: ghzhang_ustb@163.com; ORCID: https://orcid.org/0000-0003-1786-035X

powders had a significant effect on the densification of Mo-1wt% Ni, and the oxygen content in the range of 0.3 at% to 0.6 at% can promote the activation sintering process. LEE et al [12] produced spherical Mo grains by sintering the fine molybdenum powder mixed with a large amount of fine nickel powder, and the change of grain shape was observed. It was exhibited that the liquid phase sintered Mo-Ni alloy presented a typical alloy structure with isotropic solid-liquid interfacial energy. PANICHKINA et al [13] investigated the sintering kinetics of molybdenum powder and activated sintering mechanism of molybdenum with nickel addition. Because of the high solubility of Mo in Ni, Mo atoms can rapidly diffuse to the sintering neck and form a "short-circuit" mass transport path, while the reverse solubility of Ni in Mo was low, which ensures that the liquid will not flow rapidly, thus enhancing the densification. GERMAN et al [14, 15] reported that the addition of effective sintering additives, such as Pd, Pt, Ni, Co, or Fe, increased the self-diffusion of Mo, vastly improved the sintering rate, and reduced the sintering temperature. The decrease of sintering temperature can delay the growth of grain, give full play to the long-term sintering benefit of activator, and beneficially yield fully dense molybdenum-based cermets with excellent performances.

Although adding appropriate amount of nickel to Mo alloys can activate sintering and accelerate densification, it has been plagued by brittle phase. The inadequate ductility is a well-known bottleneck limiting the extensive engineering application of molybdenum alloys [16 − 18]. Relevant work revealed that the diffusion rate of Mo in $\delta$-MoNi compound is about $3\times10^{-10}$ cm$^2$/s at 1280 °C [19], which is 26000 times that of pure Mo ($1.15\times10^{-14}$ cm$^2$/s). At the same time, the formation of the brittle intermetallic compound $\delta$-MoNi is very fast and exists stably at the grain boundary of sintered compact. In addition, its coefficient of thermal expansion (CTE) is much higher than that of pure molybdenum, resulting in the fact that the brittleness of intermetallic compounds cannot be eliminated [20]. Although Mo-Ni alloy has a high sintering density (relative density>95.5%) and high hardness (HV 310 for Mo-1.5 wt% Ni and HV 110 for pure Mo [20]), the bending strength of Mo-1.5 wt% Ni alloy obtained by liquid phase sintering is only 340 MPa which is far lower than that of pure Mo compacts with the relative density of 82.1% (605 MPa) [20]. In addition, the fracture surface of Mo-Ni compacts has no ductility.

In order to eliminate the brittle phase, lots of research have been done, and it was found that the binary activators containing nickel may be more effective than single nickel element in enhancing the sintering of molybdenum and improving the mechanical properties due to the formation of the second phase with a low melting point. It is universally acknowledged that tungsten and molybdenum are similar in many properties. When various combinations are added, such as Ni-Fe [21], Ni-Cu [22], Ni-Cu-Fe [23], Ni-Cr [24], Ni-Co [25] and Ni-Al [26], their effects on the sintering of W and Mo are better than the single element. JOHNSON et al [27] processed 85 wt% Mo-Cu by infiltrating pre-sintered Mo skeleton with liquid Cu. It was found that copper existed in pre-sintered Mo skeleton after sintering, which triggered the potential of various metal binders for liquid phase sintering densification of Mo [28]. HWANG et al [29] successfully enhanced the sintering of molybdenum compacts with Ni-Cu mixture, and observed that molybdenum particles had better wettability to Cu, although the compaction had no ductility. Tungsten heavy alloy (WHA) exhibits a high strength and ductility owing to the refinement of microstructure and uniform dissolution of tungsten particles in nickel based fcc ductile binder phase $\gamma$(Ni-Fe-W) [21], and the elongation of W-Ni-Fe and W-Ni-Cu alloys could exceed 10% [21]. YE et al [30] confirmed that the best mechanical properties of tungsten alloy were achieved at the Ni/Fe ratio of 7:3. LASSNER et al [31] stated that the formation of brittle intermetallic compounds can be effectively prevented when the Ni/Fe ratio is 7:3.

Based on the above findings, Fe was introduced into Mo-Ni alloy to eliminate its brittleness. So far, the Ni-Fe mixture has not been widely applied to the activation sintering of molybdenum-based alloys. The effects of different Ni/Fe ratios on sintering microstructure, morphology and mechanical properties of alloys were studied. Firstly, the ultrafine Mo-Ni-Fe composite alloy powder was synthesized by the two-step reduction process described in our previously work [32−34], with molybdenum oxide, nickel oxide and iron oxide powders as raw materials. Secondly,

Mo-Ni-Fe series alloys with different Ni/Fe ratios were prepared by powder metallurgy, and the influence of different Ni/Fe ratios on sintering microstructure, morphology and mechanical properties was investigated.

## 2 Theoretical analyses

### 2.1 Selection of sintering temperature

In order to determine the optimum sintering temperature and ensure the occurence of liquid phase sintering, the binary phase diagrams of Mo-Ni, Mo-Fe and Ni-Fe were plotted by FactSage 8.0, as shown in Figures 1(a)−(c), respectively. It is clearly found that the lowest melting point of Mo-Ni alloy occurrs at the peritectic point of 1362 °C, while the lowest melting point of Mo-Fe alloy is 1540 °C, which is significantly higher than that of Mo-Ni system. In addition, it can also be observed from the phase diagram that the solubility of Ni in Mo is only 1.9 at% at 1362 °C, while the solubility of Fe in Mo is much higher. It is worth noting that a solid solution phase $\gamma$(Ni, Fe) with a low melting point of 1440 °C presents in the Ni-Fe binary phase diagram [35]. Besides, the ductile fcc $\gamma$(Ni, Fe) phase could be uniformly distributed in the near spherical bcc tungsten particles, which constitutes the extensively studied tungsten heavy alloy [36]. As we all know, with the increase of temperature, the diffusion speed increases. Nevertheless, the accompanying grain growth rate at high temperature may far exceed the speed of pore elimination, which is not favorable to sintering densification. Therefore, to choose the suitable sintering temperature, the equilibrium phase diagram of 95Mo-Ni-Fe system was also calculated according to FactSage 8.0 as showed in Figure 1(d). It can be concluded from Figure 1(d) that liquid phase is formed in 95Mo-Ni-Fe system at 1450 °C. Therefore, the sintering temperature was determined to be 1450 °C in the current study.

### 2.2 Selection of Ni/Fe ratio

In terms of improving the sintering activity of Mo, the effect of Ni activation sintering was particularly prominent. In the case of a small amount of nickel addition, the diffusion rate of molybdenum through the nickel grain boundary layer increased, which was much faster than the volume diffusion of molybdenum, so it can be densified rapidly through the grain boundary diffusion process. However, the development of this technology was blocked by the brittleness of sintered compacts. There are two kinds of intermetallic compounds in Mo-Ni system: $Cu_3Ti$ type orthorhombic phase $\gamma$-$MoNi_3$, and orthorhombic phase $\delta$-MoNi. Brittle $\delta$-MoNi phase formed by peritectic reaction at 1362 °C, may not be

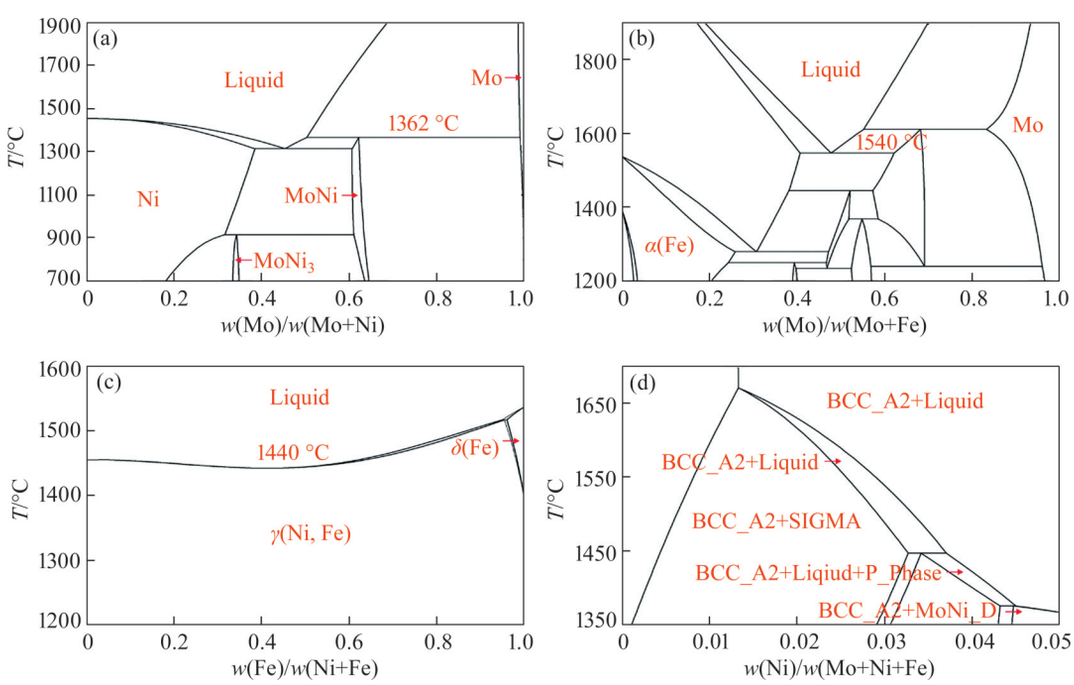


**Figure 1** Phase diagrams: (a) Mo-Ni binary phase diagram; (b) Mo-Fe binary phase diagram; (c) Ni-Fe binary phase diagram; (d) Mo-Ni-Fe phase diagram with $w$(Mo)/$w$(Mo+Ni+Fe)=0.95

eliminated during the sintering process of Mo-Ni alloy. $\gamma$-$MoNi_3$ [13, 37, 38] existed at lower temperature (about 800 °C). It was found that the reason for the brittleness and the poor ductility of the $\delta$-MoNi alloy is the effect of $\delta$-MoNi alloy on the nickel-rich thin layer surrounding the molybdenum grains [39−43]. Whether it was activation sintering or liquid phase sintering, stable intermetallic compound $\delta$-MoNi was rapidly formed in the molybdenum matrix or at the grain boundary at 1280 ℃, which covered the whole grain boundary and would not dissolve in Mo. HWANG et al [29] suggested that the formation of $\delta$-MoNi can be retarded by adjusting sintering parameters or adding other elements to change the composition and properties of brittle layer. HWANG et al [44] confirmed that the grain boundary structure of tungsten sintered by Ni doping changed from order to disorder, which accelerated the grain boundary diffusion and increased the densification.

The addition of iron in W-Ni-Fe series can reduce the melting point of the liquid phase, improve the solubility of tungsten in $\gamma$(Ni, Fe) phase and promote the sintering densification. The mechanical behaviors of W-Ni-Fe alloys were closely related with Ni/Fe ratio as well as the microstructure and densification of the alloy. The appropriate Ni/Fe ratio can not only avoid the formation of brittle intermetallic compounds, but also reduce the pores during the formation of the liquid phase. The effect of Ni/Fe ratio on the mechanical properties of the alloy has been extensively investigated, and it was worth noting that the formation of brittleness could be suppressed and the best mechanical properties of the alloy were achieved when $w$(Ni): $w$(Fe) =7: 3 [31, 45]. It was also proved that the best bonding phase structure in W-Ni-Fe tungsten heavy alloy was $\gamma$(Ni, Fe) with the crystal structure of fcc rather than bcc, $\alpha$(Ni, Fe). In conclusion, the purpose of this study is to investigate the effect of appropriate Ni/Fe ratio (including $w$(Ni): $w$(Fe) =7: 3) on the mechanical properties of Mo-Ni-Fe alloy at 1450 °C.

## 3 Experimental process

### 3.1 Preparation of ultrafine composite powder

High purity molybdenum oxide powder ($MoO_3$, 99.9% purity, Jinduicheng Molybdenum Co., Ltd., Xi'an, China), nickel oxide powder (NiO, 99.9% purity, Aladdin Industrial Co., Ltd.), iron oxide powder ($Fe_2O_3$, 99.9% purity, Sinopharm Chemical Reagent Co., Ltd.), and carbon black (MA100, Mitsubishi Chemical Corporation) were used as the raw materials. Figure 2 displays the micro-morphologies of raw materials. As can be seen from Figure 2, the $MoO_3$, NiO and $Fe_2O_3$ were micron-sized particles and carbon black was nano-sized particles. The oxide powders were mixed according to the stoichiometry of four target alloys shown in Table 1, and the amount of carbon black was determined by the content of oxide. In this

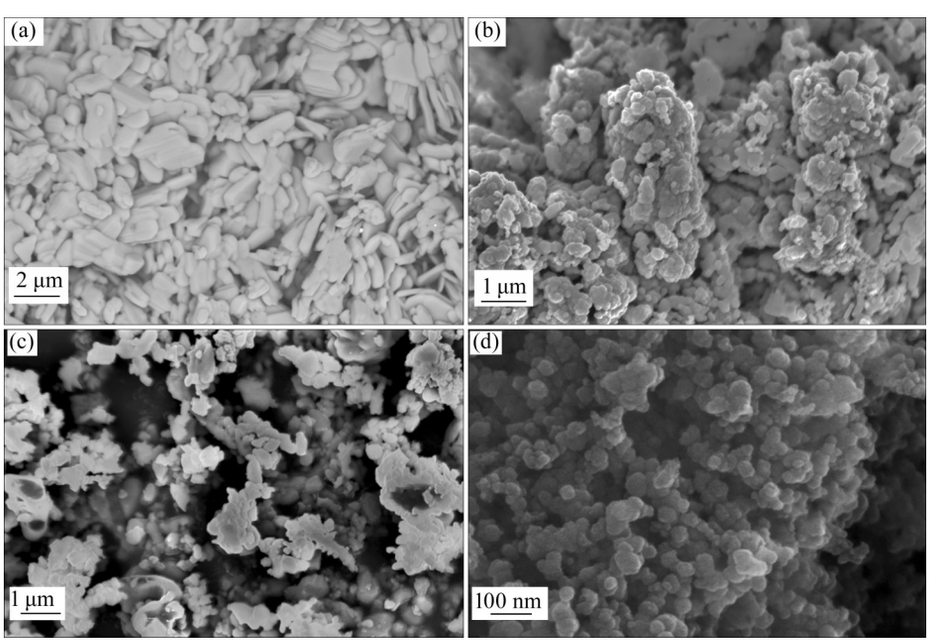


**Figure 2** FE-SEM micrograph of original powders: (a) $MoO_3$; (b) NiO; (c) $Fe_2O_3$; (d) Carbon black

**Table 1** Chemical composition of 95Mo-Ni-Fe alloy

| Alloy | Composition/wt% | | | *w*(Ni)/*w*(Fe) |
|---|---|---|---|---|
| | Mo | Ni | Fe | |
| A | 95 | 5 | 0 | 5:0 |
| B | 95 | 3.5 | 1.5 | 7:3 |
| C | 95 | 2.5 | 2.5 | 5:5 |
| D | 95 | 1.5 | 3.5 | 3:7 |

work, the molar ratio of carbon to NiO and $Fe_2O_3$ used to reduce NiO and $Fe_2O_3$ was kept at 1, and the optimum molar ratio of carbon to $MoO_3$ used to reduce $MoO_3$ was 1.9 [32−34].

The mixed powders were milled at nylon tank in anhydrous alcohol for 180 min. The planetary ball mill (QM-3SP2) was performed at a milling speed of 300 r/min with the weight ratio of ball to material of 5: 1 and the milling bodies of zirconia balls. After milling, the slurry was dried under vacuum at 70 °C for 3 h. Subsequently, these powders will be used to prepare ultrafine 95Mo-5Ni, 95Mo-3.5Ni-1.5Fe, 95Mo-2.5Ni-2.5Fe and 95Mo-1.5Ni-3.5Fe composite alloy powders.

The detailed preparation process of composite powder could be found in Refs. [46, 47]. The mixed oxide powder was first carbothermic pre-reduced in argon (Ar≥99.999%) atmosphere (400 mL/min) at 650 °C for 2 h and then at 1050 °C for 4 h. After that, the carbothermic pre-reduced powder was subjected to the deep reduction under pure hydrogen atmosphere (400 mL/min) at 800 °C for 4 h.

### 3.2 Preparation of alloy

The composite alloy powders with different compositions were pressed into rectangular strips of 32 mm×12 mm×4 mm under 200 MPa uniaxial hydraulic pressure, with the binder of 2.0 wt% stearic acid. Meanwhile, the relative density of the rectangular green compacts was about 60%. For the aim of removing the binder and oxide from compacts, the compacts were pre-sintered first at 400 °C for 2 h and then at 800 °C for 2 h in $H_2$ atmosphere. Subsequently, the sintering was carried out in a vertical tubular furnace at 1450 °C for 2 h with the heating rate of 5 °C/min. The sintering atmosphere was the flowing Ar-$H_2$ (Ar: 160 mL/min; $H_2$: 40 mL/min). After sintering, the sample was taken out from the furnace before cooling to room temperature. The surfaces of sintered samples were ground with different grades of SiC sandpaper (600−2000 ASTM size), and then polished with diamond to 1 μm to remove surface oxides and pollutants for further analysis and testing. Figure 3 shows the flowchart for the preparation of 95Mo-Ni-Fe alloy.

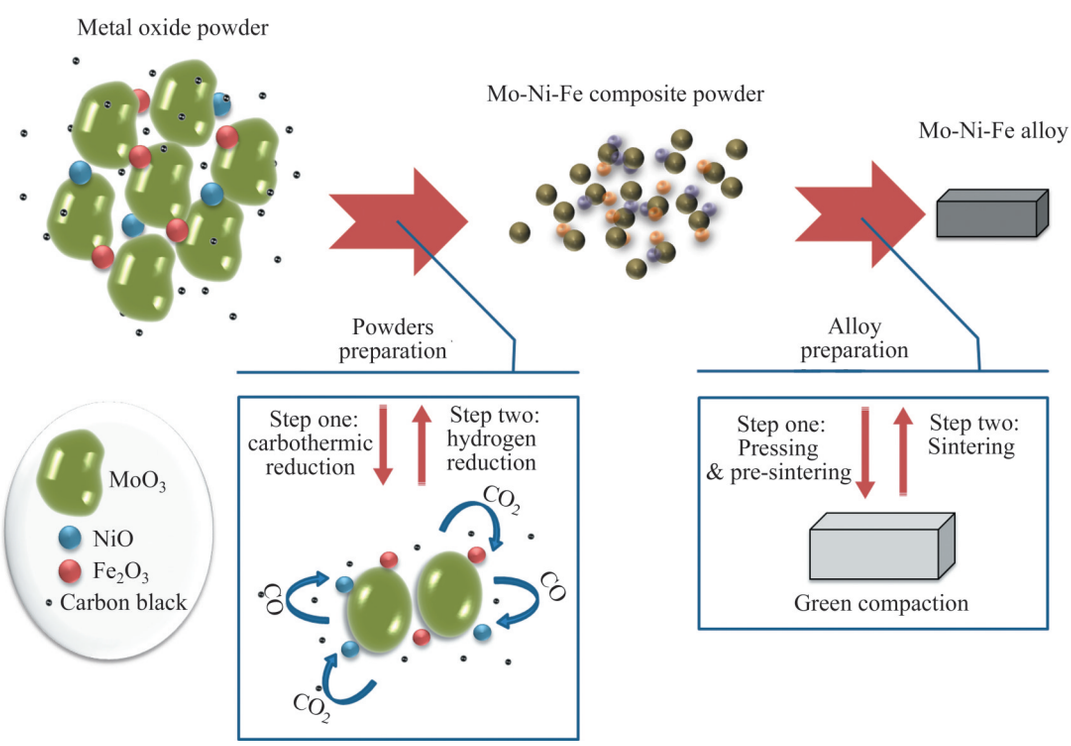


**Figure 3** Flowchart for preparation of 95Mo-Ni-Fe alloy

### 3.3 Performance test and microstructure characterization

The apparent density of the sample was measured with Archimedes techniques, and the relative density of the samples was calculated by combining the theoretical densities of four samples (10.22, 10.18, 10.15 and 10.07 g/cm$^3$). Hardness measurements were carried out using a Vickers hardness tester (THV-1MDX) by applying 50 g load for 10 s. The bending strength was measured at room temperature using three-point bending method on specimens with the dimensions of 12 mm× 3 mm×2 mm. The tests were carried out at a cross-head speed of 0.5 mm/min in a testing machine (CDW-5, Changchun Chaoyang Test Instrument Ltd., China). The following formula was used to calculate the bending strength:

$$R = \frac{3FL}{2bh^2} \quad (1)$$

where $R$ is bending strength, and its value is the maximum stress that the material can bear before it breaks or reaches the specified bending moment under the bending load; $F$ is the maximum fracture load (N); $L$ is the span length for the three-point bending test (mm); $b$ is the width (mm), and $h$ is the height (mm).

In this study, the span of three-point bending test sample is 7 mm. The phase composition of the reduction products and sintered compacts was determined by the X-ray diffraction (TTR III, RIGAKU Corporation, Japan) using Cu $K_\alpha$ radiation ($\lambda$=0.15406 nm) in the range of $2\theta$=10°−90° with a scanning rate of 10°/min. The morphology of alloy powders was characterized by a field emission scanning electron microscope (FE-SEM, Zeiss SUPRA 55, Oberkoche, Germany), and an energy dispersive X-ray spectroscope (EDS) was used to analyze elemental composition. The cross section and bending fracture structure of the as-sintered bodies were observed by scanning electron microscopy (SEM, ZeissEVO-18, Germany) incorporated with energy dispersive spectroscopy (EDS).

## 4 Results and discussion

### 4.1 Analysis of 95Mo-Ni-Fe alloy powders with different Ni/Fe ratios

Taking the preparation of 95Mo-2.5Ni-2.5Fe composite powder as an example, the XRD results of powders after carbothermic reduction and the following deep hydrogen reduction are shown in Figure 4(a). The X-ray diffraction patterns of carbothermic pre-reduction product showed that there was a small amount of incomplete reduction oxide, which is vitally important for reducing the residual carbon content [32 − 34]. After hydrogen reduction, the diffraction peaks of oxides in the products disappeared, and the Mo-Ni-Fe composite powder with Mo as main phase was obtained. The diffraction peak intensities of other phases are relatively weak ascribing to the small contents of iron and nickel. Figures 4(b) and 5 illustrate the XRD results and the microstructure of the composite powders observed by FE-SEM, respectively. It can be seen from Figure 4(b) that the raw materials are completely reduced to Mo-Ni-Fe composite powder. With the increase of the

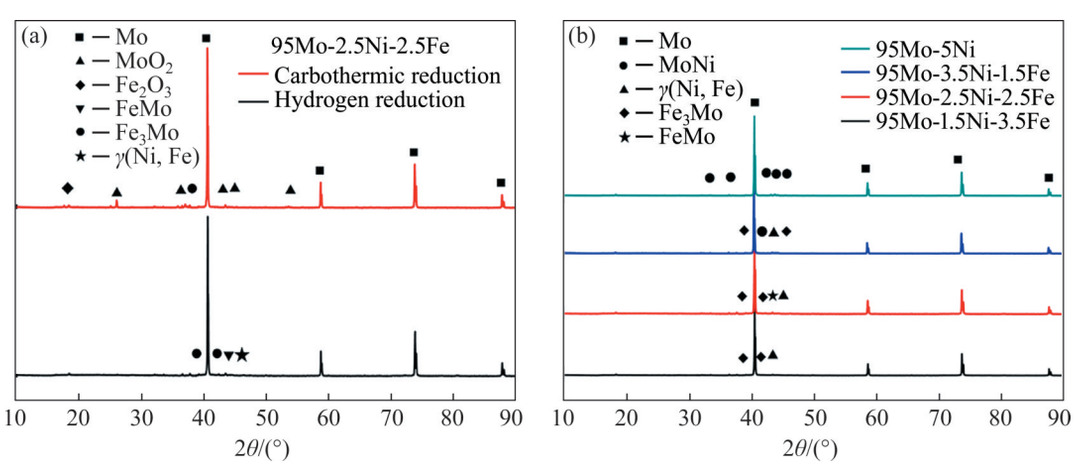


**Figure 4** (a) XRD spectrum of 95Mo-2.5Ni-2.5Fe product powder after carbothermic reduction and hydrogen reduction; (b) XRD spectrum of composite alloy powder after two-step reduction

substitution proportion of Fe for Ni, $\gamma$(Ni, Fe), $Fe_3Mo$ and FeMo phases were revealed [48]. Besides the Mo phase with the strongest diffraction peaks in the product, only MoNi phase can be observed in 95Mo-5Ni. As some Ni was replaced by Fe, there are MoNi, $\gamma$(Ni, Fe) and $Fe_3Mo$ phases in alloy B; $\gamma$(Ni, Fe), $Fe_3Mo$ and FeMo phases in alloy C; $\gamma$(Ni, Fe) and $Fe_3Mo$ in alloy D. The distribution of different elements in 95Mo-3.5Ni-1.5Fe (alloy B) composite powder was analyzed by EDS. It can be observed from Figure 6 that after deep hydrogen reduction, Ni and Fe particles were evenly distributed in the molybdenum matrix of 95Mo-3.5Ni-1.5Fe sample.

The morphology images of composite alloy powders after carbothermic reduction and hydrogen reduction are shown in Figure 5. All composite powders were composed of large Mo grains and fine ferronickel grains adhered on Mo grains. It can be seen from Figure 5 that there was a slight sintering in the carbothermic reduction product attributing to the existences of Ni and Fe, and there is no obvious change after hydrogen reduction. After the addition of Fe, the agglomeration and activation sintering of

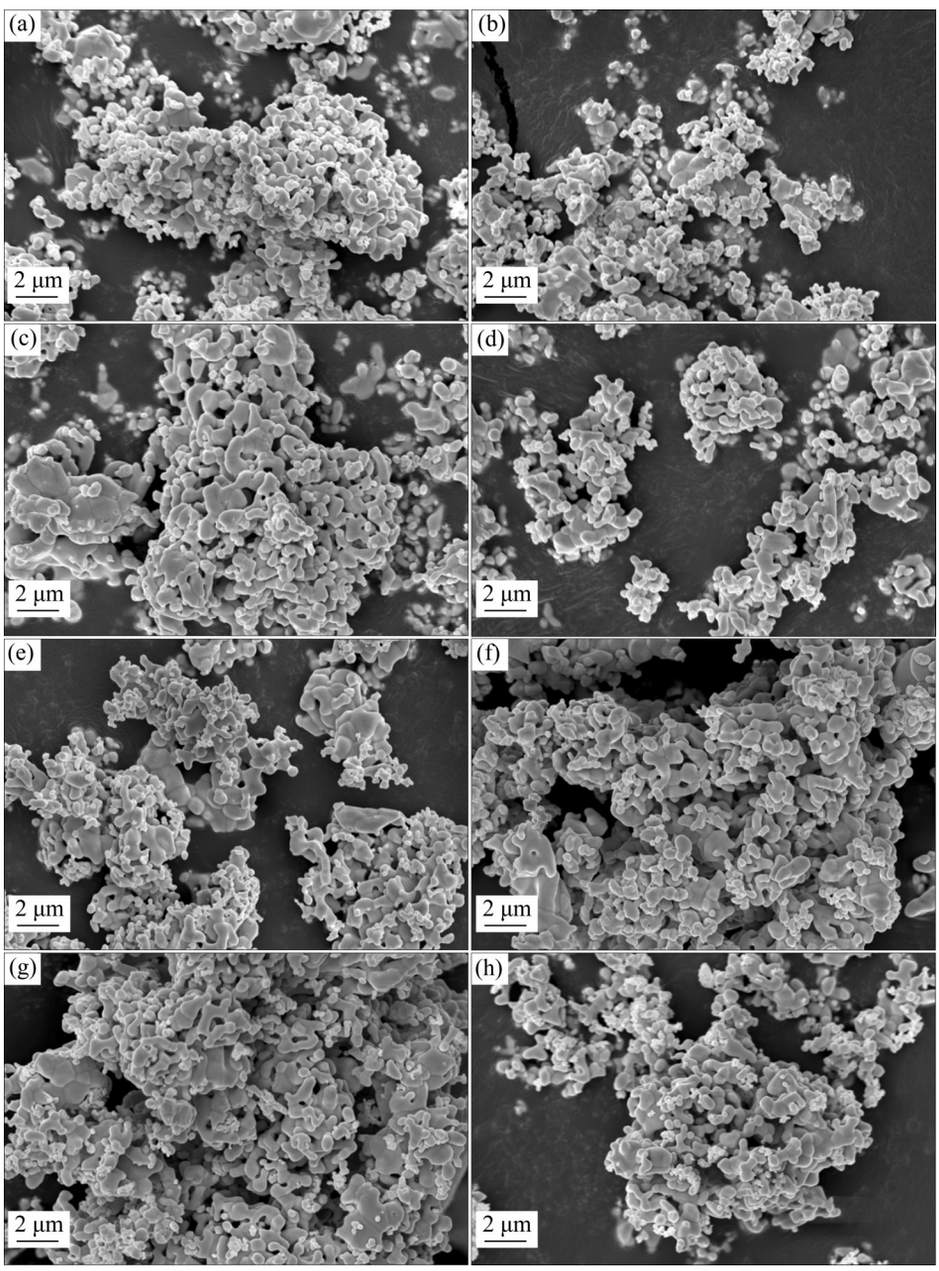


**Figure 5** Micro morphology of powder after carbothermic reduction of (a) 95Mo-5Ni, (b) 95Mo-3.5Ni-1.5Fe, (c) 95Mo-2.5Ni-2.5Fe and (d) 95Mo-1.5Ni-3.5Fe; Micro morphology of powder after hydrogen reduction of (e) 95Mo-5Ni, (f) 95Mo-3.5Ni-1.5Fe, (g) 95Mo-2.5Ni-2.5Fe and (h) 95Mo-1.5Ni-3.5Fe

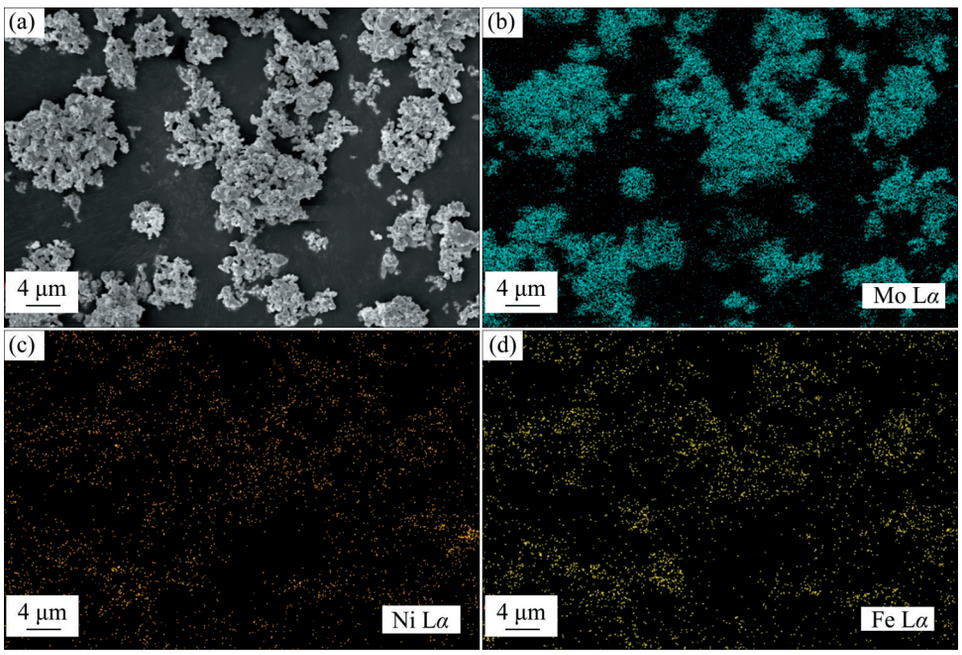


**Figure 6** (a) SEM of 95Mo-1.5Ni-3.5Fe composition powder; EDS analyses of (b) Mo, (c) Ni and (d) Fe

molybdenum particles are significant. Considering that nickel and iron are easy to form a variety of intermetallic compounds with molybdenum (as shown in Figure 4(b)), they have a synergistic activation sintering effect on molybdenum.

### 4.2 Effect of different Ni/Fe ratios on densification behavior of 95Mo-Ni-Fe alloy

Table 2 compares the change of relative density of the four alloys sintered at 1450 °C for 2 h. Obviously, the relative densities of all samples were above 98.74%. The curve of thermal dilatometer shows that Ni is the best activator and the addition of Fe has little contribution to the relative density [23]. The addition of nickel has a positive effect on the liquid phase sintering of molybdenum, which is mainly ascribed to the sufficient dissolution of Mo in Ni, good wettability and chemical compatibility. SMITH [49] investigated the sintering kinetics of Mo-0.5−0.75wt% Ni, and found that the diffusion of Mo through Ni surface layer was about two orders of magnitude larger than the molybdenum volume self-diffusion. Therefore, nickel can strengthen the diffusion of molybdenum and form dense materials through liquid phase sintering.

From the micrograph of the alloy powder (Figure 5), it can be seen that during the solid-state heating process of the mixed powder at 1050 °C, Ni and Fe played a role of co-activation sintering.

**Table 2** Relative density of 95Mo-Ni-Fe alloys with different Ni/Fe ratios sintered at 1450 °C for 2 h (%)

| Alloy A | Alloy B | Alloy C | Alloy D |
|---|---|---|---|
| 99.43 | 98.74 | 99.13 | 98.81 |

Subsequently, during the sintering process at 1450 °C, the solid particles agglomerated to form skeletons, which restrained the liquid phase diffusion and affected the densification. As increasing the proportion of Fe, the formation temperature of the liquid phase increased, and the diffusion rate slowed down, which was unfavorable to complete densification. So, the relative densities of alloys B, C and D after sintering at 1450 °C were lower than that of Mo alloy only containing Ni.

Figures 7 and 8 show the XRD results and cross-section morphologies of sintered 95Mo-Ni-Fe alloys with different Ni/Fe ratios. The XRD result shown in Figure 7 indicates that after sintering, there are intermetallic compounds in Mo-Ni-Fe alloy, which are different from Mo-Ni-Fe composite powder. From the nearly spherical molybdenum grains in Figure 8, it could be deduced that liquid phase sintering occurred obviously in alloys A, B and C. To further examine the element distribution of the alloy, the EDS analysis of 95Mo-2.5Ni-2.5Fe was carried out, with the results shown in Figure 9 and Table 3. The existences of small grains in the

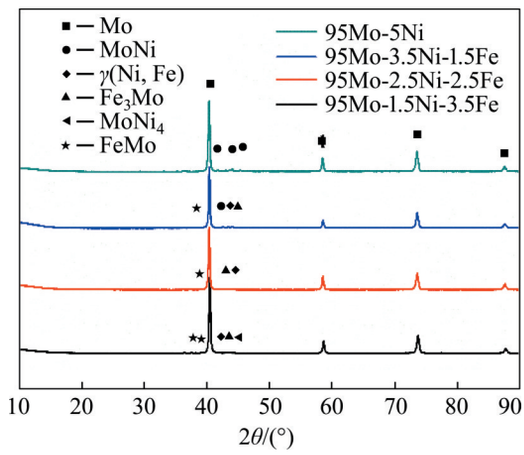


**Figure 7** Phase compositions of 95Mo-Ni-Fe alloys with different Ni/Fe ratios sintered at 1450 °C for 2 h

binder phases of alloys B and C indicated that during the cooling process, a small amount of Mo grains dissolved in binder were re-precipitated from the binder phase.

The densification process of 95Mo-Ni-Fe system may be described as follows: At the initial stage of sintering, as the temperature increases, the liquid phase is formed. Solid Mo grains could be partially wetted in the liquid phase, which provides "shortrange diffusion path" to pull solid grains adhere, grains rearrange and densify rapidly. In the middle sintering stage, the rapid densification occurs mainly by particle rearrangement in liquid phase. However, when Ni is replaced by Fe, the formation temperature of liquid phase increases, and thus the densification rate is slowed down. In the later stage of sintering, as rearrangement process slows down, liquid phase sintering enters into solution re-precipitation stage again. Meanwhile, solution re-precipitation is accompanied by grain coarsening. The smaller size of Mo grains has the higher solubility in the surrounding liquid phase. As a result, the small grains disappear while the large grains grow up gradually, and thus the average size becomes larger. In the subsequent sintering process, it is difficult for the closed microporosity to be completely removed. So, compared with alloy A, relative densities of alloys B, C and D are smaller. However, although nickel makes molybdenum alloy denser than iron, nickel promotes grain growth more rapidly than iron [10]. Consequently, the grain size of alloy D is the smallest.

### 4.3 Effect of different Ni/Fe ratios on mechanical properties of 95Mo-Ni-Fe alloy

The effect of Ni/Fe ratios on the hardness and bending strength of 95Mo-Ni-Fe alloy is shown in Figure 10. The alloy A has the highest relative density (99.43%, Table 2), the lowest hardness (HV 423.8) and the lowest bending strength

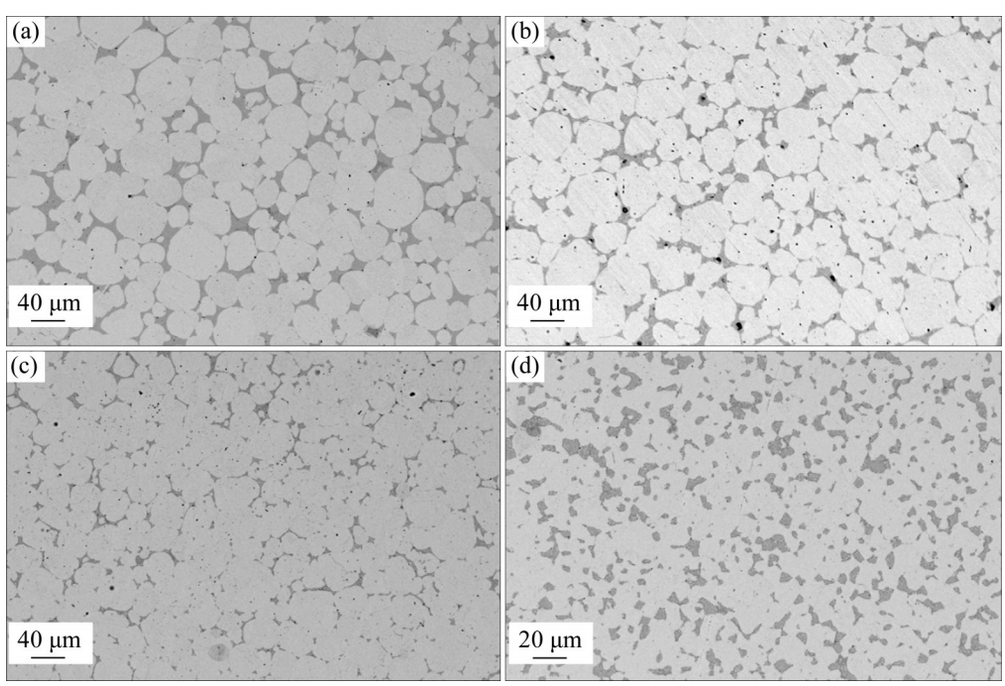


**Figure 8** Cross section morphology of 95Mo-Ni-Fe alloys with different Ni/Fe ratios sintered at 1450 °C for 2 h: (a) 95Mo-5Ni; (b) 95Mo-3.5Ni-1.5Fe; (c) 95Mo-2.5Ni-2.5Fe; (d) 95Mo-1.5Ni-3.5Fe

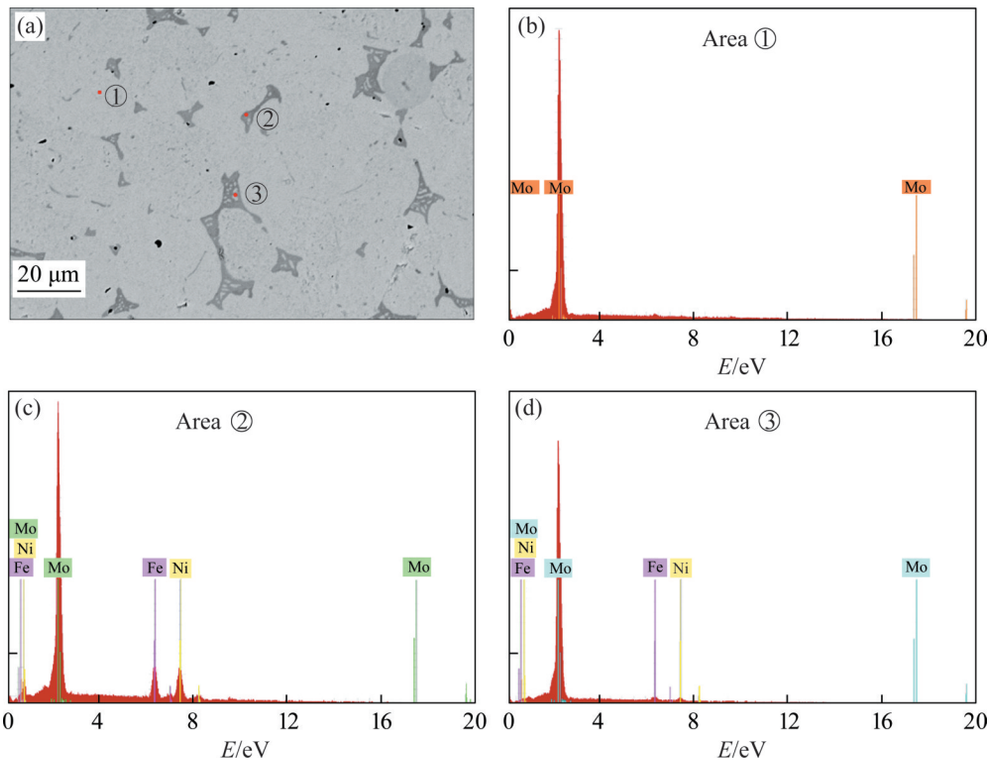


**Figure 9** EDS image of sintered 95Mo-2.5Ni-2.5Fe alloy

**Table 3** EDS results of different areas in Figure 9 (at%)

| Region | Mo | Ni | Fe | Total |
|---|---|---|---|---|
| ① | 100 | — | — | 100 |
| ② | 55.39 | 26.26 | 18.35 | 100 |
| ③ | 90.30 | 4.65 | 5.06 | 100 |

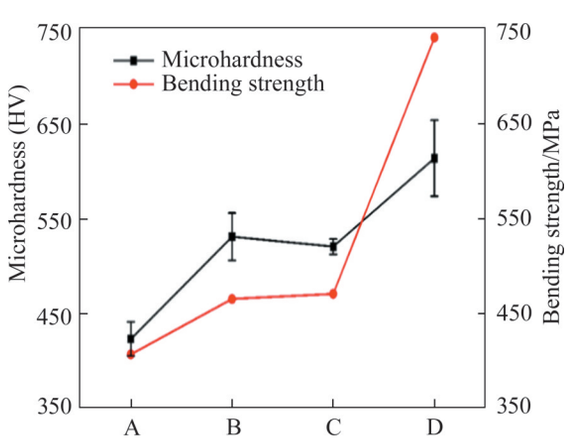


**Figure 10** Changes of density, hardness and bending strength of 95Mo-Ni-Fe alloys A–D sintered at 1450 °C for 2 h

(407.56 MPa). The reason is that the brittle intermetallic compound $\delta$-MoNi is inevitably formed in Mo-Ni alloy. Based on the conclusion of HWANG et al [20], the hardness and bending strength were HV 310 and 340 MPa for the Mo-1.5 wt% Ni, respectively. The higher hardness and bending strength in the current study are probably caused by the smaller grain size of molybdenum. With the increase of the substitution content of Fe for Ni, the hardness tends to increase, but there is a small decrease for alloy C. The hardness of the alloy mainly depends on the binder content, the binder structure and the average grain size of Mo. Therefore, the increase of hardness of alloy B, C and D is ascribed to the reduction of brittle phase. Meanwhile, the cause of the smaller hardness of alloy C than that of alloy B is attributed to different binders. The activation sintering effect of Fe is inferior to that of Ni, which slows down the densification and grain growth of Mo. Consequently, the average grain size of Mo in alloy D is the smallest, resulting in a higher hardness of HV 614 than alloys B and C.

The bending strengthes of alloys B, C and D are 465.84, 471.26 and 741.07 MPa, respectively, and with the decrease of Ni/Fe ratio, the bending strength increases. One reason is that ductile $\gamma$(Ni, Fe) phase generates and brittle $\delta$-MoNi phase decreases at the grain boundary. Different binder phase structure is conducive to the formation of disordered grain boundary structure, which

increases the grain boundary strength between Mo grains. Second, the alloy with small grain size has a high bending strength according to the Hall-Petch equation [50]. So, the bending strength of the 95Mo-Ni-Fe alloy is higher than that of 95Mo-Ni, which is consistent with the variation trend of hardness. The decrease of brittle $\delta$-MoNi compound in alloy C makes the bending strength slightly higher than that of alloy B. It can be seen from Figure 8(d) that the grain size of the alloy D is the smallest, which makes it have the highest bending strength. Relative to the low bending strength (418 MPa) of Mo-1Ni-0.5Fe sintered at 1300 °C for 1 h [17], a high content of binder phase is the main reason for the high bending strength in this work.

### 4.4 Effect of different Ni/Fe ratios on fracture mode of 95Mo-Ni-Fe alloys

Figure 11 illustrates the fracture surface of 95Mo-Ni-Fe alloys with different Ni/Fe ratios. For 95Mo-5Ni with brittle phase (as shown in Figure 11(a)), its fracture mode is obviously intergranular fracture. These fracture surfaces are primarily intergranular failure between molybdenum grains, accompanied by a small quantity of fracture between molybdenum grains and binder phase. The analysis shows that the brittle intermetallic compound $\delta$-MoNi [20, 29] is formed at the grain boundary of the sample. That is also the reason for the decrease of bending strength.

With the decrease of Ni/Fe ratio, the brittle phase in the binder phase is obviously reduced as indicated in Figure 7. The transgranular and intergranular fractures can be observed in Figures 11(b) and (c). For alloy D, the fracture is mainly in the form of trans-granular cleavage of the Mo grain (as shown in Figure 11(d)). The grain sizes of alloys B and A are the similar, while the brittle phase is reduced in alloy B relative to alloy A. The fracture surface of alloy B tends to Mo grain intergranular failure and Mo grain-binder phase interfacial dissociation. The grain size of alloy C decreases obviously and the proportion of grain boundary increases (Figure 11(c)), which means that the fracture mode needs to take a circuitous path. The main fracture modes include the interface failure between molybdenum grains and binder phase, the ductile tearing of binder phase, and a small amount of Mo cleavage. For alloy D, the grain size is refined and there is almost no brittle phase in the binder phase. The fracture surface shows lots of trans-granular fracture of molybdenum grains in addition to small amounts of Mo grain-binder phase interfacial dissociation, which is often related to the highest fracture toughness.

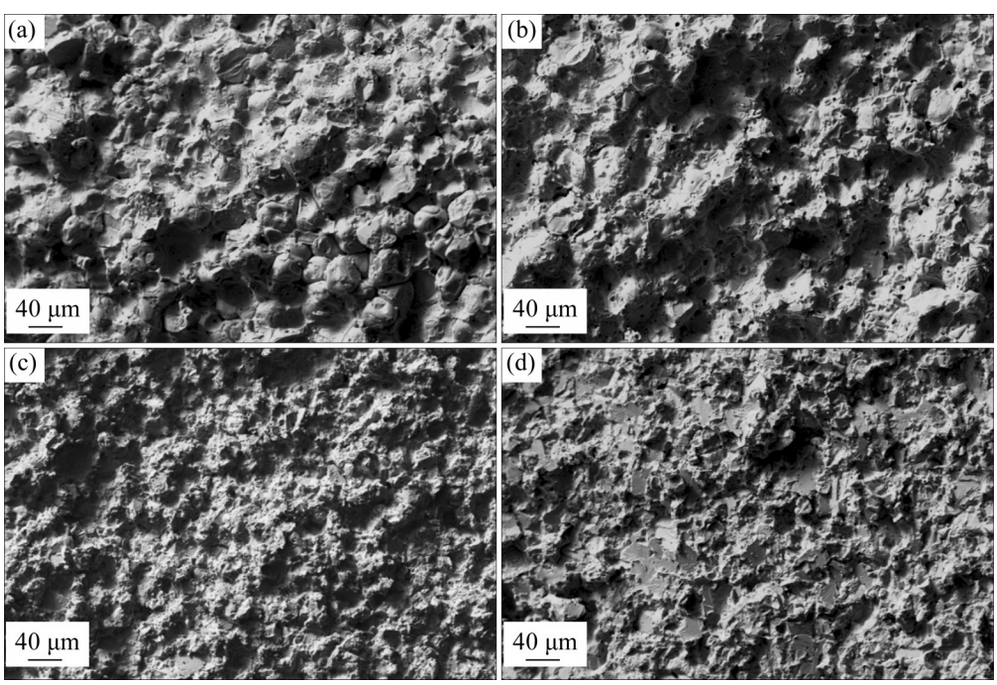


**Figure 11** Fracture surface morphology of 95Mo-Ni-Fe alloys with different Ni/Fe ratios sintered at 1450 °C for 2 h: (a) 95Mo-5Ni; (b) 95Mo-3.5Ni-1.5Fe; (c) 95Mo-2.5Ni-2.5Fe; (d) 95Mo-1.5Ni-3.5Fe

## 5 Conclusions

1) Ultrafine 95Mo-Ni-Fe composite alloy powder (<2 μm) was prepared by carbothermic pre-reduction and then hydrogen deep reduction. And then 95Mo-Ni-Fe alloy was obtained by liquid phase sintering at 1450 °C.

2) The hardness and bending strength of Mo-Ni-Fe alloy with different Ni/Fe ratios are higher than those of 95Mo-5Ni alloy. The results show that 95Mo-1.5Ni-3.5Fe alloy has the highest hardness value (HV 614) and the highest bending strength value (741 MPa).

3) After adding Fe, the fracture mode of the alloy changes from intergranular fracture to combination of intergranular and transgranular fracture. In particular, the grain refinement of 95Mo-1.5Ni-3.5Fe alloy is effective, and the fracture mode is Mo cleavage.

## Contributors

LIU Jun-ru, ZHANG Guo-hua and CHOU Kuo-chih developed the overarching research goal. LIU Jun-ru, LI Zhi-bo and CHEN Ben conducted the experiments, analyzed the test data, and wrote the initial draft of the manuscript.

## Conflict of interest

LIU Jun-ru, LI Zhi-bo, CHEN Ben, CHOU Kuo-chih and ZHANG Guo-hua declare that they have no conflict of interest.

## References

[1] MADAY M F, GIORGI R, DIKONIMOS-MAKRIS T. Correlations between the electrochemical behaviour and surface film composition of TZM alloy exposed to divertor water coolant environments [J]. Journal of Nuclear Materials, 1997, 246(1): 70−76. DOI: 10.1016/S0022-3115(97)00020-2.

[2] DIMIDUK D M, PEREPEZKO J H. Mo-Si-B alloys: Developing a revolutionary turbine-engine material [J]. MRS Bulletin, 2003, 28(9): 639−645. DOI: 10.1557/mrs2003.191.

[3] EL-GENK M S, TOURNIER J M. A review of refractory metal alloys and mechanically alloyed-oxide dispersion strengthened steels for space nuclear power systems [J]. Journal of Nuclear Materials, 2005, 340(1): 93 − 112. DOI: 10.1016/j.jnucmat.2004.10.118.

[4] KASERER L, BRAUN J, STAJKOVIC J, et al. Fully dense and crack free molybdenum manufactured by Selective Laser Melting through alloying with carbon [J]. International Journal of Refractory Metals and Hard Materials, 2019, 84: 105000. DOI: 10.1016/j.ijrmhm.2019.105000.

[5] LIU G, ZHANG G J, JIANG F, et al. Nanostructured high-strength molybdenum alloys with unprecedented tensile ductility [J]. Nature Materials, 2013, 12(4): 344 − 350. DOI: 10.1038/nmat3544.

[6] GARG P, PARK S J, GERMAN R M. Effect of Die compaction pressure on densification behavior of molybdenum powders [J]. International Journal of Refractory Metals and Hard Materials, 2007, 25(1): 16 − 24. DOI: 10.1016/j.ijrmhm.2005.10.014.

[7] ZOVAS P E, GERMAN R M. Retarded grain boundary mobility in activated sintered molybdenum [J]. Metallurgical and Materials Transactions A, 1984, 15(6): 1103 − 1110. DOI: 10.1007/BF02644704.

[8] GERMAN R M, MUNIR Z A. Heterodiffusion model for the activated sintering of molybdenum [J]. Journal of the Less Common Metals, 1978, 58(1): 61 − 74. DOI: 10.1016/0022-5088(78)90071-1.

[9] GERMAN R M, RABIN B H. Enhanced sintering through second phase additions [J]. Powder Metallurgy, 1985, 28(1): 7−12. DOI: 10.1179/pom.1985.28.1.7.

[10] ZOVAS P E, GERMAN R M, HWANG K S, et al. Activated and liquid-phase sintering—Progress and problems [J]. JOM, 1983, 35(1): 28−33. DOI: 10.1007/BF03338181.

[11] HOFMANN H, GROSSKOPF M, HOFMANN-AMTENBRINK M, et al. Sintering behaviour and mechanical properties of activated sintered molybdenum [J]. Powder Metallurgy, 1986, 29(3): 201 − 206. DOI: 10.1179/pom.1986.29.3.201.

[12] LEE D D, KANG S J L, YOON D N. A direct observation of the grain shape accommodation during liquid phase sintering of Mo-Ni alloy [J]. Scripta Metallurgica et Materialia, 1990, 24(5): 927−930. DOI: 10.1016/0956-716X(90)90139-8.

[13] PANICHKINA V V, SKOROKHOD V V, KHRIENKO A F. Activated sintering of tungsten and molybdenum powders [J]. Soviet Powder Metallurgy and Metal Ceramics, 1967, 6(7): 558−560. DOI: 10.1007/BF00774073.

[14] GERMAN R M. Sintering theory and practice [M]. New York: Wiley-Interscience, 1996.

[15] GERMAN R M, SURI P, PARK S J. Review: Liquid phase sintering [J]. Journal of Materials Science, 2009, 44(1): 1 − 39. DOI: 10.1007/s10853-008-3008-0.

[16] WADSWORTH J, NIEH T G, STEPHENS J J. Recent advances in aerospace refractory metal alloys [J]. International Materials Reviews, 1988, 33(1): 131−150. DOI: 10.1179/imr.1988.33.1.131.

[17] COCKERAM B V. The fracture toughness and toughening mechanism of commercially available unalloyed molybdenum and oxide dispersion strengthened molybdenum with an equiaxed, large grain structure [J]. Metallurgical and Materials Transactions A, 2009, 40(12): 2843−2860. DOI: 10.1007/s11661-009-9919-9.

[18] SCHNEIBEL J H, BRADY M P, KRUZIC J J, et al. On the improvement of the ductility of molybdenum by spinel ($MgAl_2O_4$) particles [J]. Zeitschrift Für Metallkunde, 2005, 96(6): 632−637. DOI: 10.3139/146.101081.

[19] ASKILL J. Tracer diffusion data for metals, alloys, and simple oxides [M]. New York: Plenum Press, 1970.

[20] HWANG K S, HUANG H S. Identification of the segregation layer and its effects on the activated sintering and ductility of Ni-doped molybdenum [J]. Acta Materialia, 2003, 51(13): 3915 − 3926. DOI: 10.1016/S1359-6454(03)00216-7.

[21] CHURN K S, GERMAN R M. Fracture behavior of W-Ni-Fe heavy alloys [J]. Metallurgical Transactions A, 1984, 15(2): 331−338. DOI: 10.1007/BF02645119.

[22] HUBER A, SIGL L S. On the sintering of molybdenum with two liquid phases [J]. Materialia, 2020, 9: 100600. DOI: 10.1016/j.mtla.2020.100600.

[23] HWANG K S, HUANG H S. Ductility improvement of Ni-added molybdenum compacts through the addition of Cu and Fe powders [J]. International Journal of Refractory Metals and Hard Materials, 2004, 22(4, 5): 185−191. DOI: 10.1016/j.ijrmhm.2004.06.003.

[24] SAKAMOTO T. Effect of Ni-Fe and Ni-Cr alloys addition on sintering of molybdenum powders [J]. Journal of the Japan Society of Powder and Powder Metallurgy, 1997, 44(7): 689−693. DOI: 10.2497/jjspm.44.689.

[25] PRABHU G, KUMAR R A, NANDY T K. Effect of cyclic heat treatment on the microstructure and mechanical properties of W-Ni-Co alloys [J]. International Journal of Refractory Metals and Hard Materials, 2019, 82: 31 − 42. DOI: 10.1016/j.ijrmhm.2019.03.024.

[26] SAKAMOTO T, HONDA T, MIURA H, et al. Effect of Ni and $Ni_3Al$ additions on sintering of molybdenum powders [J]. Materials Transactions, JIM, 1997, 38(4): 326−333. DOI: 10.2320/matertrans1989.38.326.

[27] JOHNSON J L, GERMAN R M. Role of solid-state skeletal sintering during processing of Mo-Cu composites [J]. Metallurgical and Materials Transactions A, 2001, 32(3): 605−613. DOI: 10.1007/s11661-001-0077-y.

[28] JOHNSON J L, GERMAN R M. Solid-state contributions to densification during liquid-phase sintering [J]. Metallurgical and Materials Transactions B, 1996, 27(6): 901 − 909. DOI: 10.1007/s11663-996-0003-1.

[29] HWANG K S, HUANG H S. The liquid phase sintering of molybdenum with Ni and Cu additions [J]. Materials Chemistry and Physics, 2001, 67(1 − 3): 92 − 100. DOI: 10.1016/S0254-0584(00)00425-9.

[30] YE Lei, HAN Yong, FAN Jing-lian, et al. Fabrication of ultrafine-grain and great-performance W-Ni-Fe alloy with medium W content [J]. Journal of Alloys and Compounds, 2020, 846: 156237. DOI: 10.1016/j.jallcom.2020.156237.

[31] LASSNER E, SCHUBERT W. Tungsten: properties, chemistry, technology of the element, alloys, and chemical compounds [M]. New York: Kluwer Academic, 1999. DOI: 978-0-306-45053-2.

[32] WANG Da-hang, SUN Guo-dong, ZHANG Guo-hua. Preparation of ultrafine Mo powders via carbothermic pre-reduction of molybdenum oxide and deep reduction by hydrogen [J]. International Journal of Refractory Metals and Hard Materials, 2018, 75: 70 − 77. DOI: 10.1016/j.ijrmhm.2018.04.002.

[33] SUN Guo-dong, ZHANG Guo-hua, CHOU K C. An industrially feasible pathway for preparation of Mo nanopowder and its sintering behavior [J]. International Journal of Refractory Metals and Hard Materials, 2019, 84: 105039. DOI: 10.1016/j.ijrmhm.2019.105039.

[34] ZHANG He, LI Zhi-bo, ZHANG Guo-hua, et al. A novel method for preparing ultrafine molybdenum powder [J]. International Journal of Refractory Metals and Hard Materials, 2021, 96: 105491. DOI: 10.1016/j.ijrmhm. 2021. 105491.

[35] SWARTZENDRUBER L J, ITKIN V P, ALCOCK C B. The Fe-Ni (iron-nickel) system [J]. Journal of Phase Equilibria, 1991, 12(3): 288−312. DOI: 10.1007/BF02649918.

[36] BOSE A, SIMS D, GERMAN R M. Test temperature and strain rate effects on the properties of a tungsten heavy alloy [J]. Metallurgical Transactions A, 1988, 19(3): 487 − 494. DOI: 10.1007/BF02649263.

[37] FRISK K. An experimental and theoretical study of the phase equilibria in the Fe-Mo-Ni system [J]. Metallurgical Transactions A, 1992, 23(2): 639 − 649. DOI: 10.1007/BF02801181.

[38] ZHOU S H, WANG Y, JIANG C, et al. First-principles calculations and thermodynamic modeling of the Ni-Mo system [J]. Materials Science and Engineering A, 2005, 397(1, 2): 288−296. DOI: 10.1016/j.msea.2005.02.037.

[39] HIRAOKA Y, OGUSU T, YOSHIZAWA N. Decrease of yield strength in molybdenum by adding small amounts of Group VIII elements [J]. Journal of Alloys and Compounds, 2004, 381(1, 2): 192 − 196. DOI: 10.1016/j.jallcom.2004.03.112.

[40] HEIJLEGEN G P, RIECK G D. Diffusion in the Mo-Ni, Mo-Fe and Mo-Co slstems [J]. Acta Metallurgica, 1974, 22(10): 1269−1281. DOI: 10.1016/0001-6160(74)90140-0.

[41] MIL'MAN Y V, RISTIĆ M M, GRIDNEVA I V, et al. Structure and hardness of sintered Mo-Ni alloys [J]. Soviet Powder Metallurgy and Metal Ceramics, 1987, 26(2): 144 − 148. DOI: 10.1007/BF00794133.

[42] SAKAMOTO T, NISHIDA M, OKAZAKI K. Microstructure of Mo powders sintered with Ni and $Ni_3Al$ powders [J]. Journal of the Japan Society of Powder and Powder Metallurgy, 1999, 46(12): 1221 − 1225. DOI: 10.2497/jjspm.46.1221.

[43] CHOU T C, LINK L. Solid-state interdiffusion in Ni-Mo diffusion couples at high temperatures [J]. Scripta Materialia, 1996, 34(5): 831 − 838. DOI: 10.1016/1359-6462(95)00601-X.

[44] HWANG N M, PARK Y J, KIM D Y, et al. Activated sintering of nickel-doped tungsten: Approach by grain boundary structural transition [J]. Scripta Materialia, 2000, 42(5): 421−425. DOI: 10.1016/S1359-6462(99)00344-9.

[45] YU Yang, REN Chao-yuan, ZHANG Wen-cong. Compressive behavior of liquid phase sintered 90 W-7Ni-3Fe heavy alloy at high temperature and low strain rate condition [J]. International Journal of Refractory Metals and Hard Materials, 2018, 76: 149−157. DOI: 10.1016/j.ijrmhm.2018.06.006.

[46] LI Zhi-bo, ZHANG Guo-hua, CHOU K C. Densification behavior of ultrafine W-Ni-Fe composite powders produced by a two-stage reduction process [J]. Powder Technology, 2020, 360: 430−443. DOI: 10.1016/j.powtec.2019.11.019.

[47] KENEL C, DAVENPORT T, LI X, et al. Kinetics of alloy formation and densification in Fe-Ni-Mo microfilaments extruded from oxide- or metal-powder inks [J]. Acta

Materialia, 2020, 193: 51−60. DOI: 10.1016/j.actamat.2020.04.038.
[48] RAJKUMAR V B, HARI KUMAR K C. Thermodynamic modeling of the Fe-Mo system coupled with experiments and *ab initio* calculations [J]. Journal of Alloys and Compounds, 2014, 611: 303−312. DOI: 10.1016/j.jallcom.2014.05.030.
[49] SMITH J T. Diffusion mechanism for the nickel-activated sintering of molybdenum [J]. Journal of Applied Physics, 1965, 36(2): 595−598. DOI: 10.1063/1.1714036.
[50] HALL E O. The deformation and ageing of mild steel: III discussion of results [J]. Proceedings of the Physical Society Section B, 1951, 64(9): 747−753. DOI: 10.1088/0370-1301/64/9/303.

**(Edited by ZHENG Yu-tong)**

## 中文导读

### Ni/Fe比对钼镍铁合金活化烧结及力学性能的影响

**摘要：**为了改善Mo-Ni合金的低塑性，在合金中加入Fe，并研究了Ni/Fe质量比对合金致密化行为、组织演变和力学性能的影响。结果表明，在95Mo-5Ni合金中加入Fe，可避免晶界处脆性金属中间相$\delta$-MoNi的形成，同时在烧结过程中也可以有效抑制Mo的晶粒长大。但是由于Ni的活化效果优于Fe，Fe的加入降低了合金的致密化程度。实验结果显示：95Mo-1.5Ni-3.5Fe合金的硬度和抗弯强度最高，分别为HV 614和741 MPa。结合弯曲断裂机理分析，相对于Mo-Ni合金，性能的改善可能归因于抑制脆性相的形成。

**关键词：**Mo-Ni-Fe合金；烧结行为；脆性相；致密化